

Effect of annealing on the crystal structure and dielectric properties of $\text{Ba}_{0.6}\text{Sr}_{0.4}\text{TiO}_3$ thick films

L.Z. Cao^a, Q.D. Meng^b, W.Y. Fu^a, S.F. Wang^{a,c}, M. Lei^a,
B.L. Cheng^a, Y.L. Zhou^{a,*}, Z.H. Chen^a

^aBeijing National Laboratory for Condensed Matter Physics, Institute of Physics, Chinese Academy of Sciences, Beijing 100080, China

^bElectronic Information Engineering College, Henan University of Science and Technology, Luoyang 471003, China

^cPhysics & Technology College, Hebei University, Baoding 071002, China

Received 31 August 2006; received in revised form 21 December 2006; accepted 28 December 2006

Abstract

$\text{Ba}_{0.6}\text{Sr}_{0.4}\text{TiO}_3$ (BST) films with different thickness were grown on (001) MgO substrates by pulsed laser deposition. Effects of thickness and post-deposition annealing on the crystal structure and dielectric properties of BST films are investigated. Enhancement of the crystal structure through post-deposition annealing is analyzed from the viewpoint of energy minimization principle of stable state. The best dielectric properties are obtained for the 500-nm-thick BST film with post-deposition annealing at 1000 °C in flowing O_2 atmosphere. Based on the high-quality BST film, a distributed microwave phase shifter was fabricated, and promising high-frequency device performance is achieved.

© 2007 Elsevier B.V. All rights reserved.

PACS: 77.55.+f; 68.55.JK; 81.40.Ef; 77.22.Ch

Keywords: (Ba,Sr)TiO₃ film; Dielectrics properties; Thickness; Heat treatment; Epitaxial growth; Phase shifter

1. Introduction

$\text{Ba}_{1-x}\text{Sr}_x\text{TiO}_3$ (BST- x) films have been considered as a suitable material for tunable microwave devices such as phase shifters, filters, and infrared detectors [1–4]. It is well known that considerable thickness is necessary for BST- x film in the practical microwave device application. However, the crystal and epitaxial properties of the film decline when its thickness reaches a certain value. Decrease of orientation degree often leads to a decrease of dielectric constant and tunability of the film, which will deteriorate the performance of microwave device. It has been demonstrated that post-deposition annealing was an effective method to improve the dielectric behavior of BST- x films [5,6]. Knauss et al. [7] reported the effect of post-deposition annealing on the crystal structure and

dielectric properties of BST- x thin films ($x = 0.35$ – 0.65). They found that annealing resulted in decrease in lattice parameter and improvement of the dielectric properties of the films. Moreover, various methods such as electron beam, laser, millimeter wave, and ultraviolet ray have been investigated to the annealing process in order to improve the dielectric properties of the films [6,8–11]. However, few researchers focus on the effect of annealing on BST- x thick films.

In this letter, we investigate the effect of thickness and post-deposition annealing on the crystal structure and dielectric properties of $\text{Ba}_{0.6}\text{Sr}_{0.4}\text{TiO}_3$ (BST) films. Mechanism of the phenomena is analyzed from the viewpoint of energy minimization principle of stable state. The best dielectric performance is obtained for the 500-nm-thick BST film with post-deposition annealing at 1000 °C in flowing O_2 atmosphere. Based on this film, a distributed phase shifter was successfully developed and its microwave performance is presented.

*Corresponding author. Tel.: +86 10 82648108; fax: +86 10 82648108.
E-mail address: ylzhou@aphy.iphy.ac.cn (Y.L. Zhou).

2. Experiments

BST target for our experiment was synthesized by conventional ceramic-sintered processing [12,13]. BST films with varied thickness were grown by pulsed laser deposition (PLD) on (001) MgO single-crystal substrates at 800 °C in an O₂ ambient pressure of 30 Pa. A 308 nm XeCl excimer laser was used with laser energy density of 2 J/cm². 500-nm-thick BST films were annealed at 1000 °C in flowing O₂ for 10 h, and it is necessary to note that the flowing O₂ was still applied during the cooling process.

The film thickness was measured by a surface profiler of Dektak 8. X-ray diffractions (XRD) θ - 2θ scan, ω scan, and ϕ scan studies were carried out to characterize the crystal and epitaxial behavior of the BST films. The surface morphologies of the BST films were observed with Nano Scope III atomic force microscopy (AFM). The dielectric behaviors of the BST film were measured by Agilent 4294A precision impedance analyzer, using the conventional interdigital electrode (IDE) method. A distributed microwave phase shifter was fabricated, the sketch of which has been described elsewhere [14]. And its microwave performance was measured using an HP 8510C network analyzer.

3. Results and discussion

Fig. 1 shows the XRD θ - 2θ scan of BST films with varied thickness. In the XRD pattern of the 300-nm-thick BST film, only BST (001) and (002) diffraction peaks appear together with (002) peak of MgO substrate, indicating a perfect *c*-axis orientation growth of the film. However, in the pattern of 500-nm-thick sample, BST (110) and (111) diffraction peaks appear in addition to the diffraction peaks mentioned above, which reveals a deteriorated *c*-orientation growth of film.

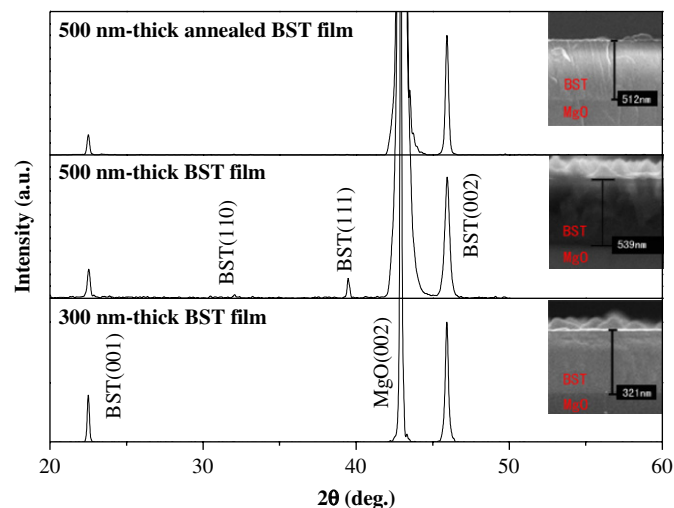


Fig. 1. XRD θ - 2θ patterns for varied thickness films: (a) 300 nm film, (b) 500 nm film, and (c) annealed 500 nm BST film. Inset is the cross-sectional microstructures of the BST films observed by SEM.

According to the energy minimization principle of stable state, total energy in film deposited on a substrate is the sum of three compositions: (1) film-substrate interface energy, (2) lattice strain energy in the film, and (3) surface energy of the film [15]. The first item can be considered as a constant for the films in our experiment because it does not depend on the thickness of the film. In the case of 300-nm-thick BST film, the strain energy due to lattice mismatch between the film and substrate dominates. Minimization of the lattice strain energy makes the deposition atoms arrangement according to the lattice pattern of the substrate, which induces the *c*-orientation growth of the films. With the increases of the thickness, the lattice strain decreases and the influence of surface energy strengthens gradually. As the thickness of the film approaches a critical value, the lattice strain energy is less than a critical value and the surface energy dominates. It is known that the grown plan with higher packing density has smaller surface energy, such as (111) and (110) plane for the BST film. Minimization of the surface energy drives the deposition atoms tending to the arrangement of high packing density. Then, the high atomic packing density arrangement fashions of the deposition atoms could appear in the grown plane of thicker films. As a result, (111) and (110) diffraction peaks are observed in the diffraction pattern of 500-nm-thick BST film, which could be attributed to the thickness effect.

In order to improve the crystal structure and dielectric behaviors of the film, the films were annealed at 1000 °C in flowing O₂ atmosphere for 10 h. After post-deposition annealing, the (110) and (111) diffraction peaks in the 500-nm-thick film disappear, which reveals the annealing process improve crystal structure of the BST film. It could be ascribed to the re-order of atomic arrangement. Reduction of the lattice strain and oxygen vacancies result in decrease of the total free energy, the effect of which restrains minimization of the surface energy. As a result, improved crystal properties were observed in the annealed 500-nm-thick BST film.

The cross-sectional microstructures of the films are shown in the inset of Fig. 1. SEM micrographs show that all of the films possess an abrupt interface between the film

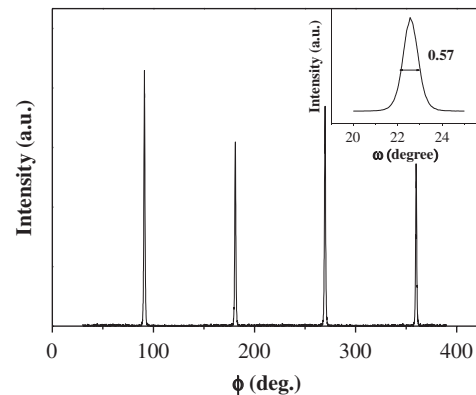


Fig. 2. ϕ scan pattern and ω -scan (inset) for annealed BST film with the thickness of 500 nm.

and substrate. Moreover, the annealed 500-nm-thick BST film exhibits a preferable surface roughness compared with the other two samples.

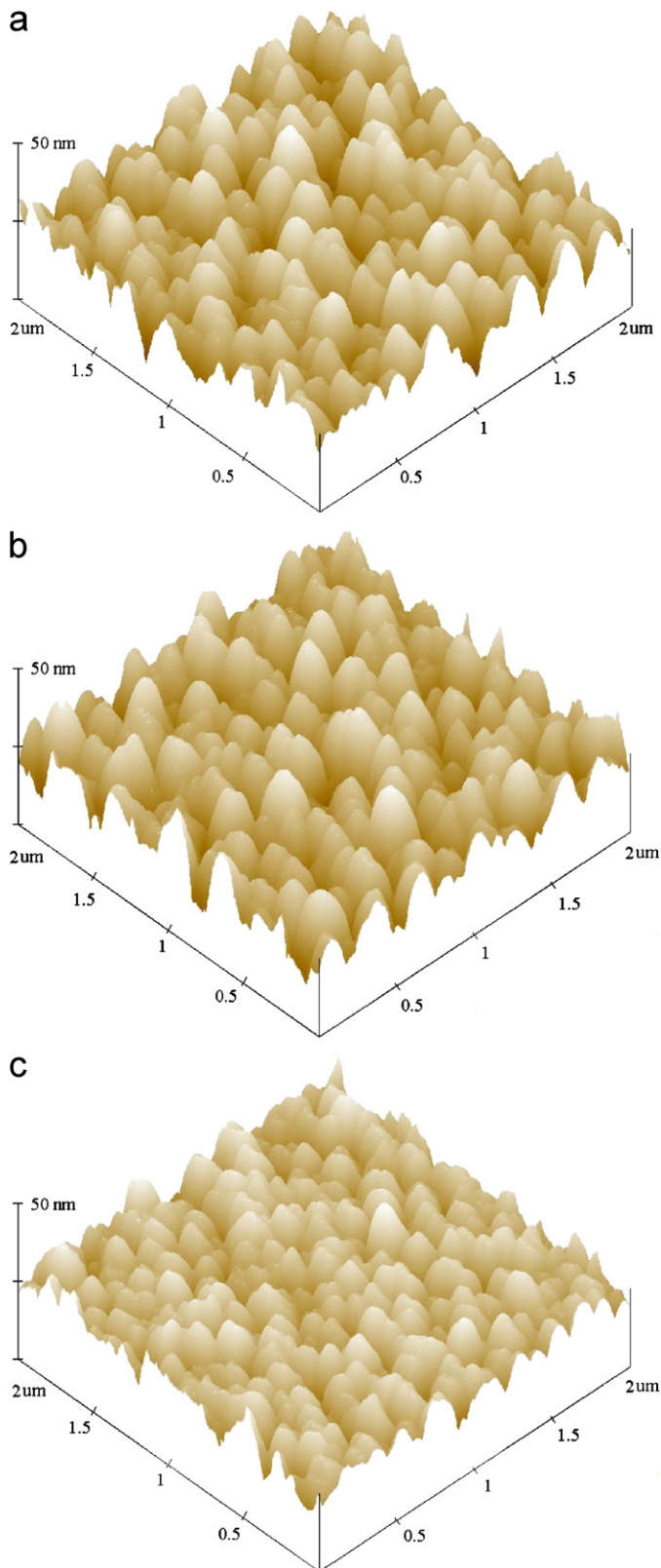


Fig. 3. AFM image for varied thickness films: (a) 300 nm film, (b) 500 nm film, and (c) annealed 500 nm BST film.

Fig. 2 shows ϕ scan pattern of BST (110) diffraction peak for annealed 500-nm-thick BST film. The scanning peaks in the pattern are spaced by 90° and no random peaks occur, which indicates that no measurable in-plane mis-orientation exists in the BST films. The rocking curve of BST film (002) peak is shown in the inset of Fig. 2, which shows a full-width at half-maximum (FWHM) value of 0.57° . The result indicates a good crystallization of annealed 500 nm BST film.

Fig. 3 shows the three-dimensional AFM images of the BST films. The AFM micrographs show that the BST films are crack free. The root-mean-square (RMS) roughness are 9.9, 10.3, and 6.4 nm for the 300, 500 nm thick, and annealed 500-nm-thick BST films, respectively. It reveals that the RMS roughness of the films has the same quantity order, even though the 500 nm film has imperfect preferred orientation. After annealing, the diffraction peaks of (111) and (110) in XRD pattern of the 500-nm-thick BST film disappear and the RMS roughness clearly reduces, which could originate from improvement of crystallization and the reduction of defect.

The bias electric field dependence of the dielectric constant and loss tangent for 500-nm-thick BST films is shown in Fig. 4. The dielectric constants at zero-bias electric field are 185 and 373 for the as-deposited and

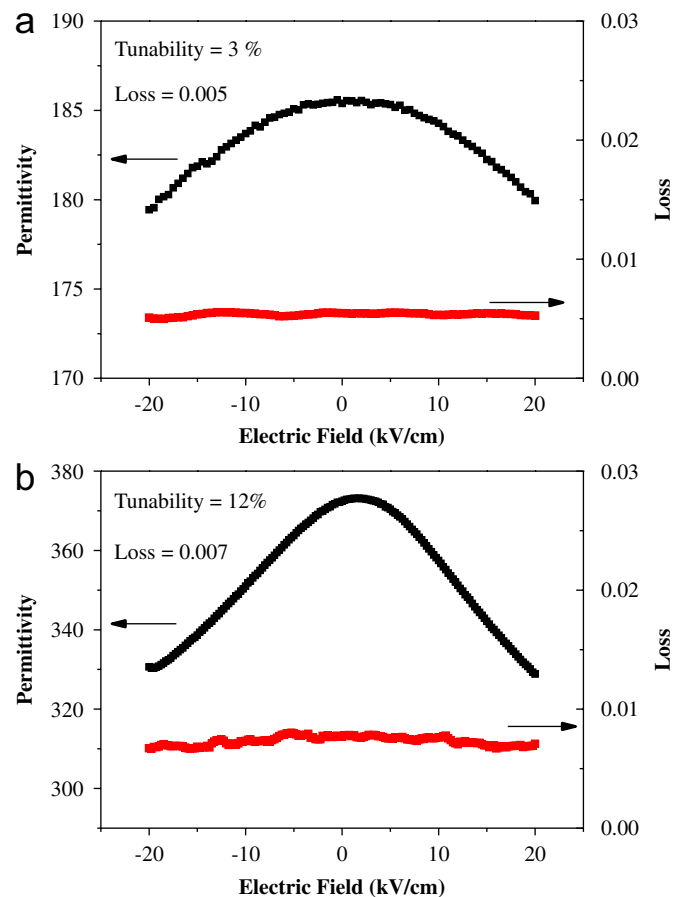


Fig. 4. Electric field dependence of dielectric constant and loss tangent for 500-nm-thick BST films: (a) as-deposited film and (b) annealed film.

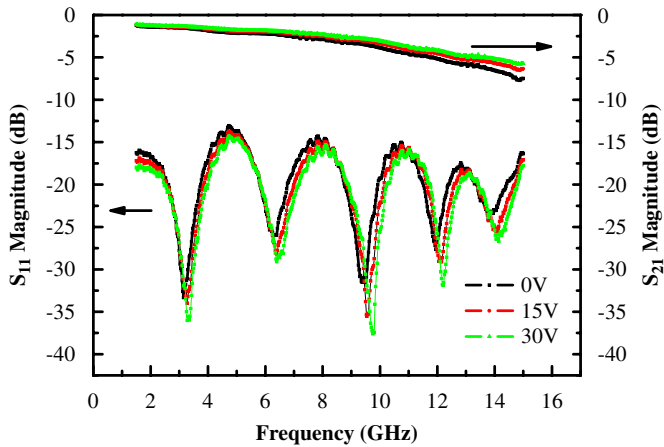


Fig. 5. Insertion loss and return loss versus frequency curves for varied DC bias voltage.

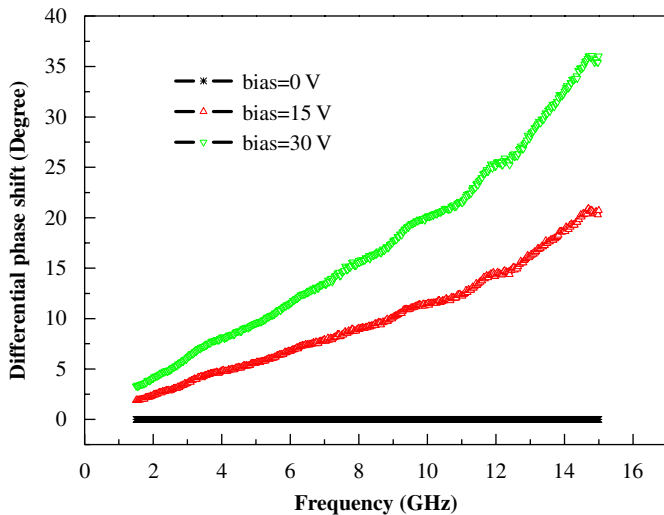


Fig. 6. Differential phase shift with different DC bias up to 30 V.

annealed films, respectively. As bias electric field 20 kV/cm applied to the sample, the tunability of 3% and 12% are observed for the as-deposited and annealed films, respectively. Although the dielectric loss increases slightly, we still can conclude that an improved crystal structure after post-annealing can results in an improved dielectric properties of the films.

Based on the annealed 500-nm-thick BST film, a distributed microwave phase shifter was successfully fabricated [14]. RF measurements are carried out on an HP 8510C network analyzer. The S-parameters of the phase shifter are recorded up to 15 GHz for different bias voltage. Fig. 5 shows that the insert loss is better than -7 dB and the return loss is under -15 dB in the range from 1.5 to 15 GHz. It is necessary to note that the return loss peak almost has the same value in the measured frequency range, which is in favor of the impedance matching. The curves of differential phase shift versus frequency for varied bias voltage are plotted in Fig. 6. The phase shift is the function of measured frequency and it rapidly increases with applied bias voltage. A moderate

differential phase shift of about 35° is observed with DC bias voltage 30 V at 15 GHz at room temperature. There is a large space for the improvement of device performance by increasing the DC bias and optimizing the circuit design.

4. Conclusion

In summary, the influence of the thickness and annealing on the crystal structure and dielectric properties of BST films has been studied. The phenomena are analyzed from the viewpoint of energy minimization principle of stable state. Excellent dielectric behaviors are observed in the 500 nm-thick BST film annealed at 1000°C in flowing O_2 atmosphere. Based on this film, a distributed phase shifter is fabricated. The insert loss of the phase shifter is better than -7 dB and the return loss is under -15 dB in the range from 1.5 to 15 GHz. And a moderate differential phase shift of about 35° is obtained with 30 V DC bias at 15 GHz.

Acknowledgments

The work is financially supported by the National Natural Science Foundation of China (60371032). The authors would like to thank X. H. Zhu for his stimulating discussions.

References

- [1] W. Chang, C.M. Gilmore, W.J. Kim, J.M. Pond, S.W. Kirchoefer, S.B. Qadri, D.B. Chirsey, J.S. Horwitz, *J. Appl. Phys.* 87 (2000) 3044.
- [2] S.K. Streiffer, C. Basceri, C.B. Parker, S.E. Lash, A.I. Kingon, *J. Appl. Phys.* 86 (1999) 4565.
- [3] A.I. Kingon, F.K. Striffer, C. Basceri, S.R. Summerfelt, *Mater. Res. Bull.* 21 (1996) 46.
- [4] F. Jin, G.W. Auner, R. Naik, N.W. Schubring, J.B. Mantese, A.B. Catalan, A.L. Micheli, *Appl. Phys. Lett.* 73 (1998) 2838.
- [5] Y.D. Xia, J.B. Cheng, B. Pan, D. Wu, X.K. Meng, Z.G. Liu, *Appl. Phys. Lett.* 87 (2005) 052902.
- [6] N. Cramer, A. Mahmud, T.S. Kalkur, *Appl. Phys. Lett.* 87 (2005) 032903.
- [7] L.A. Knauss, J.M. Pond, J.S. Horwitz, D.B. Chirsey, C.H. Mueller, R. Treece, *Appl. Phys. Lett.* 69 (1996) 25.
- [8] K. Nishizawa, T. Miki, K. Suzuki, K. Kato, *Mater. Lett.* 52 (2002) 20.
- [9] T. Zhu, Y.P. Wang, L. Zhou, Z.G. Liu, *Mater. Sci. Eng. B* 89 (2002) 390.
- [10] T. Matsumoto, H. Saito, K. Numata, S. Miyake, *Thin Solid Films* 485 (2005) 101.
- [11] M. Cervera, A. ClimentFont, J. Garrido, J. Martinez, J. Perriere, *Nucl. Instr. and Meth. B* 118 (1996) 733.
- [12] S.Y. Wang, B.L. Cheng, C. Wang, S.Y. Dai, K.J. Jin, Y.L. Zhou, H.B. Lu, Z.H. Chen, G.Z. Yang, *J. Appl. Phys.* 99 (2006) 013504.
- [13] S.Y. Wang, B.L. Cheng, C. Wang, W. Peng, S.Y. Dai, Z.H. Chen, *Key Eng. Mater.* 280–283 (2005) 81.
- [14] X.H. Zhu, Q.D. Meng, L.P. Yong, Y.S. He, B.L. Cheng, D.N. Zheng, *J. Phys. D* 39 (2006) 2282.
- [15] X.H. Zhu, H.L.W. Chan, C.L. Choy, K.H. Wong, *Appl. Phys. A* 80 (2005) 591.